ORIGINAL PAPER

Morphology studies of poly(ethylene terephthalate)/silica nanocomposites

Wentao Liu · Linlin Wu · Xingyou Tian · Jin Zheng · Ping Cui · Suqin He · Chengshen Zhu

Abstract Poly(ethylene terephthalate)/silica nanocomposites have been prepared through in situ polymerization. The morphology was investigated by atomic force microscopy in the tapping mode and scanning electron microscope. The interface morphological structure of the poly(ethylene terephthalate)/silica nanocomposites strongly depends on the ratio of silica in the matrix. When silica weight fraction is lower than 3 wt%, the system consists of aggregated silica particles dispersed in the organic matrix; beyond this concentration, the structure is co-continuous with that of the organic matrix. Surface of poly(ethylene terephthalate) was smooth; while nanocomposites were rough, there are good interfacial adhesion and compatibility between the polymer matrix and the nanofillers.

Keywords Poly(ethylene terephthalate) · Silica · AFM · SEM · Morphology

Introduction

In recent years, polymer nanocomposites have attracted extensive research interests around the world. It has been found that these materials have many advantages over traditional polymer composites with microscale fillers such as increased strength

W. Liu (✉) · L. Wu · S. He · C. Zhu
School of Materials Science and Engineering, Zhengzhou University, Daxue Road No. 75,
Zhengzhou 450052, China
e-mail: wtliu@zzu.edu.cn

X. Tian · P. Cui
The Key Laboratory of Materials Physics, Institute of Solid State Physics, CAS, Hefei 230031,
China

J. Zheng
Department of Textile Engineering, Zhongyuan Institute of Technology, Zhengzhou 450007, China

(without degrading other mechanical properties), decreased gas permeability, improved heat resistance, and enhanced electrical conductivity [1–5]. Poly(ethylene terephthalate) (PET) was first prepared in 1946 [6] and has become one of the most widely used polymer materials. Because of its low cost and high performance such as high transparency, high stability in dimension, and good mechanical properties, it can be used in a variety of fields including film, bottle, and fiber.

There are four major materials used to prepare nanocomposties with inorganic–organic properties: (a) layered clay [7–11], (b) alkoxysilane compounds as precursors and using a sol–gel technique [12–14], (c) polyhedral oligomeric silsesquioxane (POSS) molecules [15, 16], and (d) nanoparticles [17–21], nanofibers, and other synthetic materials [22]. However, owing to the poor compatibility between the organic matrix and inorganic fillers, some efforts are necessary to enhance the compatibility between the fillers and the polymer matrix during the preparation of nanocomposites. For examples, alkylammonium salts and silane coupling agents are widely used in layered clay and silica-based nanocomposites, respectively. Nanoscale colloidal silica [17], in addition to layer clay [18], has been considered as inorganic fillers for the preparation of nanocomposites associating with the sol–gel processor in situ polymerization technique. Preformed nanoscale colloidal silica has been reported to form homogeneous PMMA–silica nanocomposites with in situ PMMA polymerization and without using any coupling agents [19].

Few studies have investigated nanocomposites' morphology using atomic force microscopy (AFM) so far [23–28]. Out of three modes of AFM, tapping mode (TMAFM) is the most suitable for soft samples. In this mode, short intermittent tip sample contact reduces lateral forces, which minimizes sample damage during scanning and detects the change of surface property more sensitively.

The aim of this study was to prepare PET nanocomposites with organic-modified silica via in situ polymerization. In this study, organic-modified silica nanoparticles were dispersed in the solution of ethylene glycol monomer, and PET/silica nanocomposites were fabricated by direct polymerization. The content of silica varied from 0.5 to 5%. The surface, morphology, structure, nanofiller distribution, and performance of PET nanocomposites with different contents of silica were investigated using the TMAFM , and these results were compared to those of the scanning electron microscope (SEM) analysis of our earlier research.

Experimental

Materials

An aqueous solution of silica nanoparticles were purchased from Zhoushan MingRi Nanomaterial Limited Company, Zhejiang, ZhouShan, China. The characteristics of the aqueous solution of silica nanoparticles are summarized in Table 1 (data from the manufacturer), which shows that the sample contains 30% silica, about 70% water, and a small amount of Na_2O. The original particle size was about 10 nm.

Table 1 Summary
of nanoparticle characteristics
(data from company)

Analysis	Results
Weight percent of silica (%)	30
Particle size (nm)	12
Surface area (m^2/g)	200
Density (g/cm^3)	1.2
pH value	10
Content of Na_2O (%)	0.45

Terephthalic acid, ethylene glycol, and zinc acetate (as catalyst) were the kind courtesy of Chang Zhou Huayuan Radics Limited Company, JiangSu, China.

Preparation of PET/silica nanocomposites by in situ polymerization

PET/silica Nanocomposites were prepared by in situ polymerization. The details of the synthetic process have been described in an earlier article [29]. A series of PET/silica composites were synthesized. The contents of the silica were 0.5, 1, 3, and 5%.

Sample characterization

Atomic force microscopy observation

The specimens (of 2 mm diameter) for AFM observation were microtomed with an Ultracut Uct to 80–100 nm thick sections at −80 °C. In order to get a very smooth surface for AFM observation, the samples were first cooled by liquid nitrogen and then sliced by a diamond knife. The scanning and analysis of the samples were carried out on SPM-9500J3, Japan. The AFM measurements were carried out in air at ambient conditions (25 °C) using tapping mode probes with constant amplitude. Height and phase images were recorded simultaneously at the resonance frequency of the cantilever with a scan rate of 1 Hz and a resolution of 256 samples per line. Scanning was done at different positions of each sample, and representative images have been displayed here. Roughness measurements were done using a nanoscope image processing software.

Scanning electron microscope observation

Scanning electron microscope (FEI Sirion200 FSEM, operating with secondary electrons at 15 kV) was carried out to observe both the morphology and silica particles distribution on the fracture surface of the samples. This study investigates the fracture characteristics of these composites after rupture through impact test. Standard Izod specimens (4×10 mm^2) were fabricated by injection molding. The specimens were impact tested in a conventional pendulum-type hammer. The cross section of PET/silica nanocomposites in impact test were sputtered with a thin layer of gold for observation.

Results and discussion

Atomic force microscopy investigation

The microstructure of the two-phase PET/silica nanocomposites has been investigated by AFM. The structure features were reflected by changes in height and phase images, which have been taken at the same time. The AFM height mode image presentation is more accurate for agglomerate analysis.

The height image barely shows the valleys and hills of the surface corresponding to the dark and bright regions. The effect of silica addition on the nanocomposite structure is very visible in Fig. 1a–e. AFM images and grain size distributions clearly indicate refinement of the structure in comparison to unfilled PET (Fig. 1a). Though the AFM topography not always reveals the real surface morphology, harder surface areas might be less deformed by the tip during scanning and might appear higher in morphology images. A surface containing silica is expected to be harder in comparison with softer polymer areas. A large numer of bright areas in both the height and phase images indicate the presence of silica. In the central region of the phase images, the appearance of a valley-like depression suggests that some silica has been pulled off from the surface during sample preparation. Silica particles were homogeneously dispersed in the hybrid material matrix at low content, and the high silica content has led this hybrid material to become silica-rich. Therefore, the silica particles might approach together to exhibit silica grain shaving sizes greater than the size of the original silica (10 nm). The agglomerates are clearly visible in AFM height images (Fig. 1b–e), and their sizes are below 100 nm. Smaller crystallites are more visible in AFM phase images.

The surface roughness data of PET with different contents of silica deduced from the AFM height micrographs are showed in Table 2 and Fig. 2. According to the AFM micrographs, the silica particles were, in general, homogeneously dispersed in the PET matrix. The average surface roughness values of the PET nanocomposites films with 1 and 3% silica were estimated to be about 3.4 and 8.0 nm, respectively. It generally increased when the content of silica was increased as shown in Fig. 2, which suggests that more silica particles resided at the surfaces of the films at higher silica contents. The nanocomposite films exhibited much rougher surfaces when contents of silica were more than 3%. There might be more aggregation of the silica particles in the nanocomposite than in low silica contents films.

The AFM phase images of PET/silica nanocomposites are shown in Fig. 3. The appearance of linear silica structures was seen to be predominant with some amount of network formation also. The lengths of the linear structures run into the micronmeter range while the width varies from 10 to 20 nm. Discrete nanoscale silica particles (10–100 nm) were also dispersed throughout the matrix. According to the AFM phase images, we proposed at least part of the semicrystalline matrix is crystallized and responds like a "single crystal" Fig. 3b, c, and e.

The tablet is a "hybrid composite" surrounded by the continuous organic matrix. The inorganic phase is thus finely divided still behaving as a single crystal. It was proposed that each tablet results from the coherent aggregation of silica nanograins. The resulting phase contrasts are often difficult to interpret because of the complex
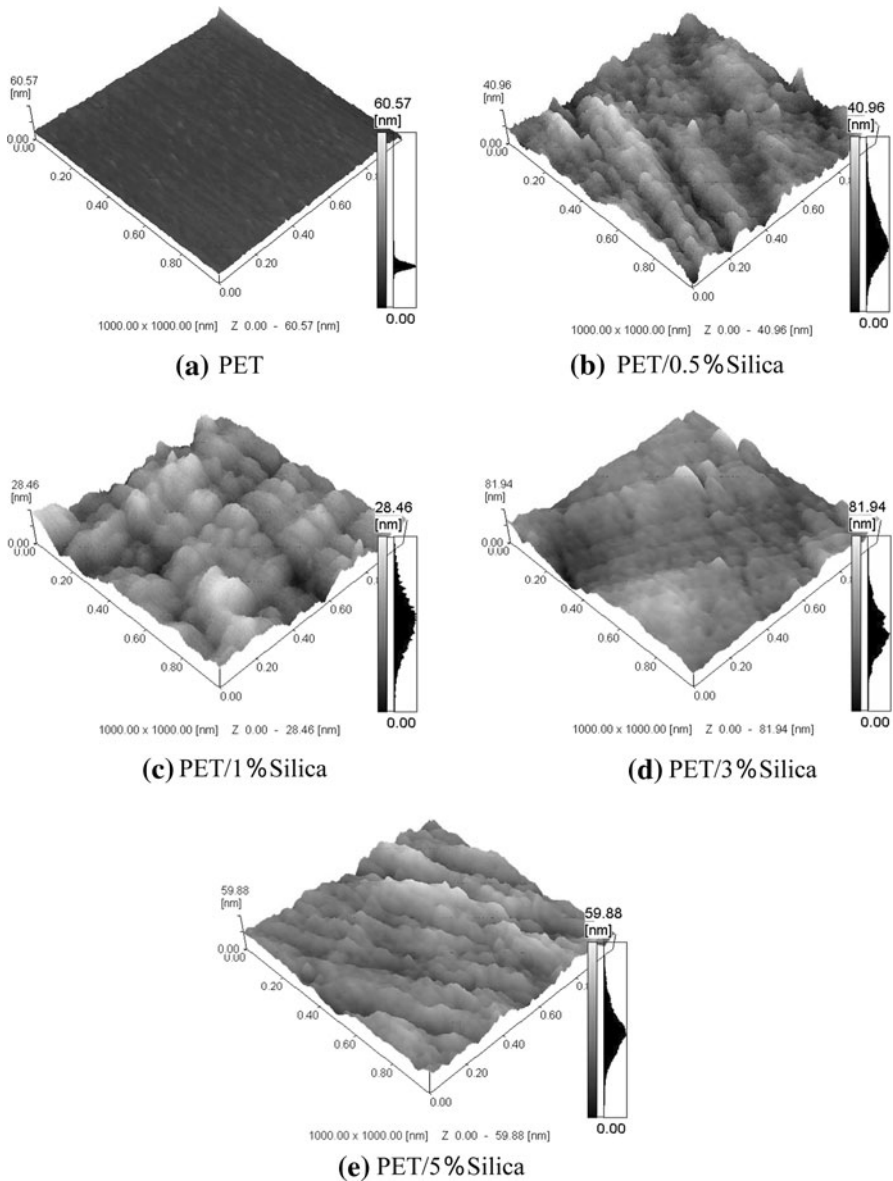
Fig. 1 AFM height images of PET/silica nanocomposites. **a** PET, **b** PET/0.5%silica, **c** PET/1%silica, **d** PET/3%silica, **e** PET/5%silica

interactions of chemical and physical effects [30, 31]. Here, the interactions can be related to the drastic difference of the elastic properties of the semicrystalline organic matrix regarding those of the inorganic phase. The organic matrix is organized as in the form of "foam" with very thin walls and closed cells as shown in

Table 2 The surface roughness of PET/silica nanocomposites

Weight percent of silica	Ra (nm)	Ry (nm)	Rz (nm)
0	1.071	34.082	12.726
0.5	5.157	45.037	20.308
1	3.472	28.493	13.819
3	8.045	76.977	37.215
5	6.107	55.778	26.535

Note: *Ra* the average surface roughness, *Rz* The average difference between five high points and low points, *Ry* the distance between the highest point and lowest point
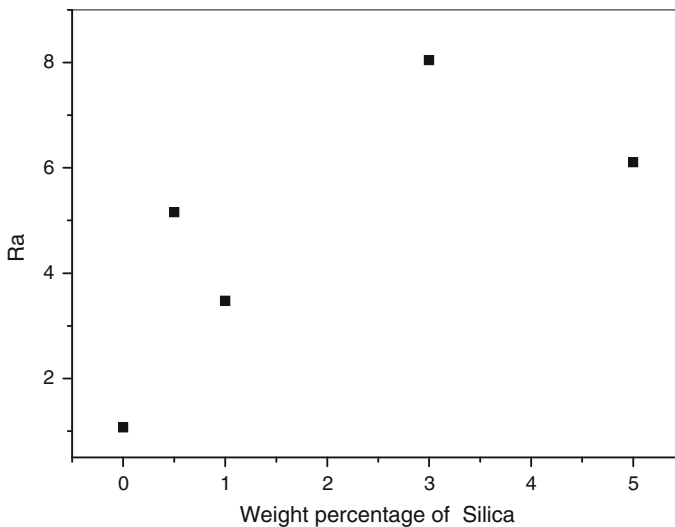

Fig. 2 Dependence of the average surface roughness (Ra) on the weight percentage of silica

Fig. 3c. All these indicate that phase separation takes place as a result of the addition of silica.

Scanning electron microscopy (SEM) observation

Images shown in Fig. 4 are ambient fractographs of the neat PET and its composites. Some differences exist between the ambient fractographs of the neat PET and the composites. Figure 4a showed that the surfaces of the pure PET samples were smooth and featureless, representing brittle failure of homogenous materials. As shown in the SEM images for the PET/silica composite samples with 0.5 and 1 wt% content of silica, the fractured surfaces were significantly different from that of pure PET samples. The fractured surfaces were broken into small and rough fractured pieces or strips, contributing to improvement of the toughness of the nanocomposites. However, the improved toughness due to the rough fractured surfaces for the cases of 3 and 5 wt% would be decreased. It resulted in the
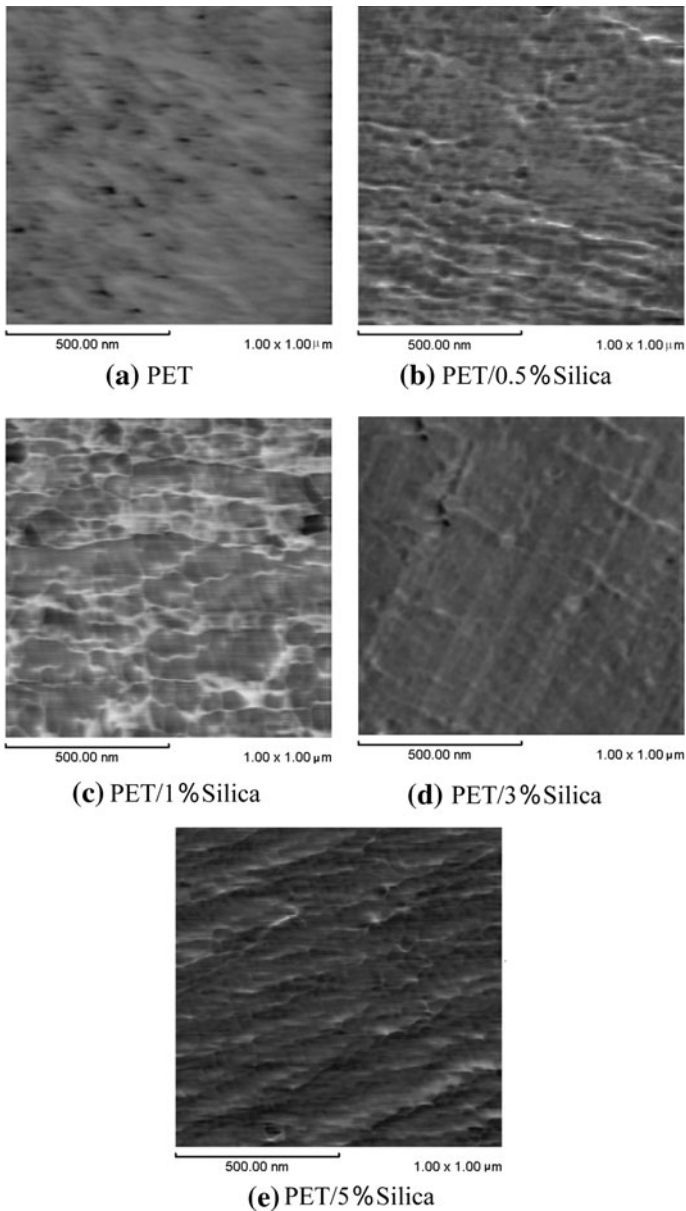
Fig. 3 AFM phase images of PET/silica nanocomposites. **a** PET, **b** PET/0.5%silica, **c** PET/1%silica, **d** PET/3%silica, **e** PET/5%silica

aggregation of silica particles, because the microcracks would relatively initiate easily at the microsized aggregated silica particles. This is probably the reason that the tensile strength and impact strength in the case of higher silica contents (3 and 5 wt%) are lower than those in the case of 1 wt% silica content as extensively found in the literature.
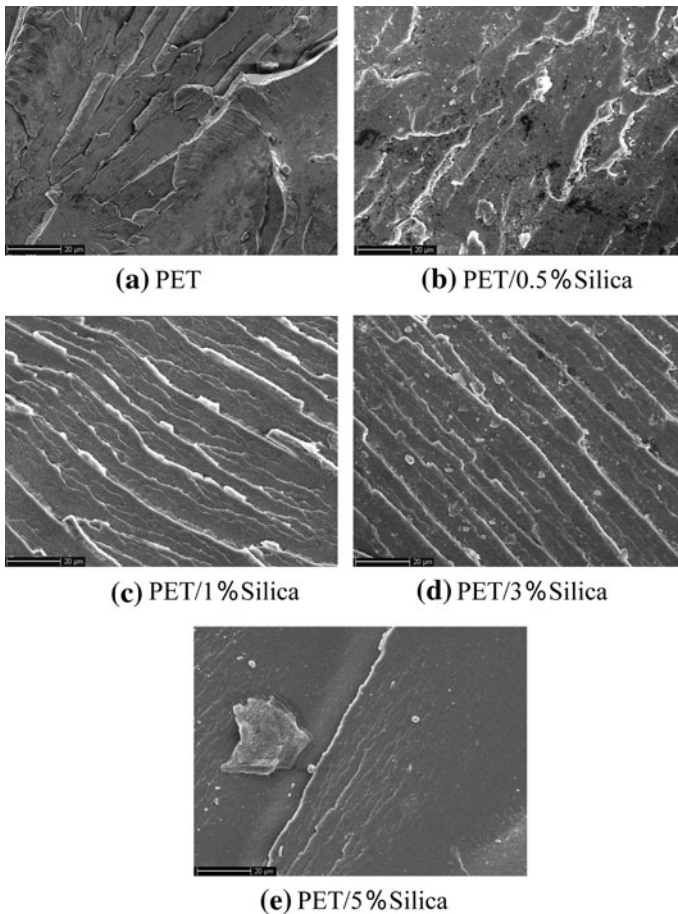
Fig. 4 SEM photographs of tensile fracture surface of PET/silica nanocomposites. **a** PET, **b** PET/
0.5%silica, **c** PET/1%silica, **d** PET/3%silica, **e** PET/5%silica

For the nanocomposite with low silica content, the fracture surface is smooth. Many parallel strips are distributed on the fracture surface of the nanocomposite when the silica content exceeds 1 wt%. Our tentative explanation is as follows. The rough fracture surface of the nanocomposites results from smaller phase separation and the special interaction between the nanoparticles and the polymer, which constrains the polymer chains' mobility and the efficiency of the rearrangement. The surface of the neat PET has brittle structures, while that of the PET/0.5 wt% silica nanocomposite (Fig. 4b) has greater toughness; when the silica content is enhanced further, the surface of the nanocomposite becomes brittle again. There are some reasons for this phenomenon: at low content, silica particles are finely dispersed in the material. There occurs good interfacial adhesion between them. While the content is enhanced, these particles become easily aggregated and debond and detach from the PET matrix due to the poor interfacial adhesion between them. Because the magnification of SEM is not very high, the dispersion of the

nanoparticles in the materials cannot be finely detected, or because the compatibility between PET and silica phase was indiscernible within the PET matrix in view of many white spots seen in the nanomaterials as in Fig. 4d.

At lower silica load, more fibrous textured morphology was formed on the fractured surface of PET. As more silica was loaded, this fibrous texture morphology became less and less, and only a slight phase separation of silica particles from PET matrix occurs. When silica was overloaded at greater than 3 wt%, PET samples became more crisp and opaque. Thus, at 5 wt% silica load, the PET got easily broken among these silica particles rather than inducing more fibers, so that more silica particles were buried in PET matrix, and they seem smaller than the particles of lower load.

Nevertheless, a good adhesion between the matrix and the silica is evident as no fracture lines are located at the interface, and also as no voids are present. Indeed, when the adhesion between the filler and the matrix is poor, the fragile fracture creates typical fracture lines at the borderline of the filler aggregates and some holes, due to the detaching of the unembedded particles are created. We can attribute, in general, this high compatibility and adhesion to the higher surface area of the silica and the good dispersion.

The compatibility between the organic polymer and silica has a great effect on the mechanical properties. In prevenient studies, we found that the impact strength of the material is the highest when the silica content is 1 wt%; the lack of plastic deformation on the fractured plane when the silica content is more than 1 wt% explains the sharp drop in the ductility of the nanocomposites in the presence of silica.

Conclusions

PET-silica nanocomposites are investigated using atomic force microscopy (AFM) in the tapping mode and SEM. The surface, morphology, structure, nanofiller distribution, and performance of pure PET and with different contents of silica were examined. The structure of the PET/silica nanocomposites strongly depends on the ratio of silica. When silica weight fraction is lower than 3 wt%, the system consists of aggregated silica particles dispersed in the organic matrix; beyond this level of the concentration of silica, the structure is co-continuous with that of the organic matrix; the pure PET samples were smooth while nanocomposites were rough. Good interfacial adhesion and compatibility between the polymer matrix and the nanofillers are caused when the content of silica is lower.

References

1. Alexandre M, Dubois P (2000) Polymer-layered silicate nanocomposites: preparation, properties and uses of a new class of materials. Mater Sci Eng R 28:1–63

2. Balazs AC (1999) Interactions of nanoscopic particles with phase-separating polymeric mixtures. Curr Opin Colloid Interface Sci 4:443–448
3. Giannelis EP (1998) Polymer-layered silicate nanocomposites: synthesis, properties and applications. Appl Organomet Chem 12:675–680
4. Soo PP, Huang BY, Jang YI, Chiang YM, Sadoway DR, Mayers AM (1999) Rubbery block copolymer electrolytes for solid-state rechargeable lithium batteries. J Electro Chem Soc 146:32–37
5. Kojima Y, Usuki A, Kawasumi M, Okada A, Fukushima Y, Kurachi T, Kamigaito O (1993) Mechanical properties of nylon 6-clay hybrid. J Mater Res 8:1185–1189
6. Whinfield JR, Dickinson JT (1946) Improvements relating to the manufacture of highly polymeric substances. UK Patent 578079
7. Wang H, Zhao T, Zhi L, Yan Y, Yu Y (2002) Synthesis of novolac/layered silicate nanocomposites by reaction exfoliation using acid-modified montmorillonite. Macromol Rapid Commun 23:44–48
8. Lepoittevin B, Pantoustier N, Devalckenaere M, Alexandre M, Kubies D, Calberg C, Jérôme R, Dubois P (2002) Poly(ε-caprolactone)/clay nanocomposites by in situ intercalative polymerization catalyzed by dibutyltin dimethoxide. Macromolecules 35:8385–8390
9. Chen C, Curliss D (2003) Processing and morphological development of montmorillonite epoxy nanocomposites. Nanotechnology 14:643–648
10. Xie W, Xie R, Pan WP, Hunter D, Koene B, Tan LS, Vaia R (2002) Thermal stability of quaternary phosphonium modified montmorillonites. Chem Mater 14:4837–4845
11. Zeng QH, Wang DZ, Yu AB, Lu GQ (2002) Synthesis of polymer-montmorillonite nanocomposites by in situ intercalative polymerization. Nanotechnology 13:549–553
12. Li C, Wilkes G (2001) Silicone/amine resin hybrid materials as abrasion resistant coatings. Chem Mater 13:3663–3668
13. Wilkes GL, Wen J, Jordens K (2000) High abrasion resistant coating material US Patent 6,072,018
14. Matejka L, Dukh O, Kolarik J (2000) Reinforcement of crosslinked rubbery epoxies by in situ formed silica. Polymer 41:1449–1459
15. Fu BX, Hsiao BS, Pagola AS, Stephens P, White H, Rafailovich M, Sokolov J, Mather PT, Jeon HG, Phillips S, Lichtenhan J, Schwab J (2001) Structural development during deformation of polyurethane containing polyhedral oligomeric silsesquioxanes (POSS) molecules. Polymer 42:599–611
16. Bharadwaj RK, Berry RJ, Farmer BL (2000) Molecular dynamics simulation study of norbornene-POSS polymers. Polymer 41:7209–7221
17. Yu YY, Chen CY, Chen WC (2003) Synthesis and characterization of organic–inorganic hybrid thin films from poly(acrylic) and monodispersed colloidal silica. Polymer 44:593–601
18. Chang CC, Wei KH, Chang YC, Chen WC (2003) Synthesis and optical properties of poly(BPDA-ODA)/silica hybrid thin films. J Polym Res 10:1–6
19. Chen WC, Lee SJ (2000) Synthesis and characterization of poly(methyl methacrylate)-silica hybrid optical thin films. Polym J 32:637–672
20. Bula K, Jesionowski T, Krysztafkiewicz A, Janik J (2007) The effect of filler surface modification and processing conditions on distribution behaviour of silica nanofillers in polyesters. Colloid Polym Sci 285:1267–1273
21. Jesionowski T, Bula K, Janiszewski J, Jurga J (2003) The influence of filler modification on its aggregation and dispersion behaviour in silica/PBT composite. Compos Interfaces 10:225–242
22. Wu TM, Liao CS (2000) Polymorphism in nylon 6/clay nanocomposites. Macromol Chem Phys 201:2820–2825
23. Li XD, Gao HS, Scrivens WA, Fei DL, Thakur V, Sutton MA, Reynolds AP, Myrick ML (2005) Structural and mechanical characterization of nanoclay-reinforced agarose nanocomposites. Nanotechnology 16:2020–2029
24. Jiang T, Wang YH, Yeh JT, Fan ZQ (2005) Study on solvent permeation resistance properties of nylon6/clay nanocomposite. Eur Polym J 41:459–466
25. Park HM, Liang XM, Mohanty AK, Misra M, Drzal LT (2004) Effect of compatibilizer on nanostructure of the biodegradable cellulose acetate/organoclay nanocomposites. Macromolecules 37:9076–9082
26. Malwitz MM, Dundigalla A, Ferreiro V, Butler PD, Henk MC, Schmidt G (2004) Layered structures of shear-oriented and multilayered PEO/silicate nanocomposite films. Phys Chem Chem Phys 6:2977–2982
27. Hu XB, Lesser AJ (2004) Enhanced crystallization of bisphenol-A polycarbonate by nano-scale clays in the presence of supercritical carbon dioxide. Polymer 45:2333–2340

28. McNally T, Murphy WR, Lew CY, Turner RJ, Brennan GP (2003) Polyamide-12 layered silicate nanocomposites by melt blending. Polymer 44:2761–2772
29. Liu WT, Tian XY, Cui P, Li Y, Zheng K, Yang Y (2004) Preparation and characterization of PET/silica nanocomposites. J Appl Polym Sci 91:1229–1232
30. Cleveland JP, Anczykowski B, Schmid AE, Elings VB (1998) Energy dissipation in tapping-mode atomic force microscopy. Appl Phys Lett 72:2613–2615
31. Tamayo J, Garcia R (1998) Relationship between phase shift and energy dissipation in tapping-mode scanning force microscopy. Appl Phys Lett 73:2926–2928